

Resonant inelastic x-ray scattering study of vector chiral ordered kagomé antiferromagnet

Zijian Xiong,¹ Trinanjan Datta,^{2,1,*} and Dao-Xin Yao^{1,†}

¹*State Key Laboratory of Optoelectronic Materials and Technologies,
School of Physics, Sun Yat-Sen University, Guangzhou 510275, China*

²*Department of Chemistry and Physics, Augusta University, 1120 15th Street, Augusta, Georgia 30912, USA*

We study the resonant inelastic x-ray scattering (RIXS) features of vector chiral ordered kagomé antiferromagnetic materials. Utilizing a group theoretical formalism that respects lattice site symmetry, we calculated the L -edge magnon contribution for the kagomé vesignieite compound $\text{BaCu}_3\text{V}_2\text{O}_8(\text{OH})_2$. In contrast to inelastic neutron scattering, we show that incoming and outgoing polarization dependence of the L -edge RIXS spectrum can be used to distinguish magnon branches. At the K -edge, we derived the two-site effective RIXS and Raman scattering operator for bimagnon excitation in vesignieite using the Shastry-Shraiman formalism. Our derivation explicitly considers spin-orbit coupling effects in virtual hopping processes. We find vector chiral correlation (four spin) contribution that is proportional to the RIXS spectrum. Our scattering operator formalism can be applied to a host of realistic non-collinear non-coplanar materials at both the L and K -edge. We demonstrate that vector chiral correlations can be accessed by current RIXS experiments.

INTRODUCTION

Chirality and magnetism can have an intimate relationship [1–4]. In geometrically frustrated spin systems [5], magnetic materials can harbor degenerate ground states [6]. The ordered magnetic phase on such a lattice can be characterized by a composite order parameter such as sublattice magnetization and vector chirality [7]. Vector spin chirality, defined as $\kappa_{ij} = \mathbf{S}_i \times \mathbf{S}_j$ where \mathbf{S}_i and \mathbf{S}_j denote spins on lattice sites i and j , signifies the rotational (clockwise or counterclockwise) sense of the non-collinear spin arrangement around a plaquette on the lattice. A vector chiral ordered state could induce the Dzyaloshinskii-Moriya (DM) interaction by the inverse DM mechanism [8–10]. Thus, to have a deeper understanding of the fundamental physics of novel frustrated magnetic phases of matter, it is necessary to study and understand the tell-tale signatures of chirality [3] and its associated chiral correlation functions. It is also worth noting that the chiral universality class has been proposed to characterize the nature of magnetic phase transition in a geometrically frustrated material [11]. The recommended phase transition classification scheme is different from an unfrustrated magnet, which is known to be in the $O(n)$ universality class.

Dzyaloshinskii-Moriya interaction exists in magnetic bonds without inversion center [12]. This favors a canted spin arrangement which can give rise to the vector and the scalar chiral order. A vector chiral ordered phase, characterized $\langle \kappa_{ij} \rangle \neq 0$, can exist in the chiral state. Moreover, the concept of scalar spin chirality $\chi_{ijk} = \mathbf{S}_i \cdot (\mathbf{S}_j \times \mathbf{S}_k)$, where \mathbf{S}_k is a spin, can be introduced to encompass the case of a non-coplanar spin arrangement. A non-coplanar arrangement is particularly important for our work which focuses on the $\mathbf{q} = \mathbf{0}$ umbrella ordered state of a kagomé lattice. In this magnetic pattern, the spins with cant out of the kagomé plane with angle η . Such a $\mathbf{q} = \mathbf{0}$ umbrella ordered state in kagomé lattice has been observed in jarosite $\text{KFe}_3(\text{OH})_6(\text{SO}_4)_2$ [7, 13], vesignieite $\text{BaCu}_3\text{V}_2\text{O}_8(\text{OH})_2$ [14, 15], Sr-vesignieite $\text{Cu}_3\text{SrV}_2\text{O}_8(\text{OH})_2$

[16, 17], edwardsite $\text{Cd}_2\text{Cu}_3(\text{SO}_4)_2(\text{OH})_6 \cdot 4 \text{H}_2\text{O}$ [18], and some variants of them. In Table I we list a collection of spin-1/2 copper based kagomé materials. Recently, kagomé materials have attracted attention due to correlation and topological effects also [19–22].

Vector (scalar) chirality correlation is described by a four (six)-spin correlation function. Virtual hopping processes are the key to accessing the multi-spin correlation channel. It was suggested that the dynamical vector chirality response, $\int dt e^{i\omega t} \langle \mathbf{S}_q(t) \times \mathbf{S}_{-q}(0) \rangle$ [23], which is a two-spin correlation function could be detected by polarized inelastic neutron scattering [24]. But, this method is limited in its scope of applicability. The technique requires an unequal number of positive and negative vector chirality domains. This makes the approach invalid for an uniform vector chirality phase, such as in jarosite $\text{KFe}_3(\text{OH})_6(\text{SO}_4)_2$. A theoretical proposal to study chirality has been made on the basis of the spin-charge-current effect [25, 26], without any possible experimental realization, yet. Additionally, multi-spin correlation functions are difficult to access unambiguously in an inelastic neutron scattering (INS) experiment [23, 24]. There have been several theoretical proposals to detect scalar chirality, too. These include Raman scattering [27, 28], INS [29], and pre-edge resonant inelastic x-ray scattering [30]. In all the above theoretical approaches, scalar spin chirality does not contribute to x-ray scattering intensity in the leading order. Thus, we focus on the dominant contribution arising from the vector chirality term.

In recent years, resonant inelastic x-ray scattering (RIXS) has rapidly developed as an useful experimental technique to probe correlated and frustrated states of matter [34–36]. It has been successfully utilized to study electronic, magnetic, orbital, and lattice excitations [37–40]. RIXS is a photon-in photon-out process, where the energy of the incoming photons are tuned to match the atomic absorption edge of specific elements in the material. Information on elementary excitations are measured by the differences between energy, momentum and polarization of the incoming and outgoing photons. The dominant contribution of the RIXS spectra at the K -edge (corresponding to a $1s \rightarrow 4p$ transition) of a Mott insulator originates from a four-spin correlation function [41]. Thus, RIXS provides an opportunity to access vector chirality. Although,

* Corresponding author: tdatta@augusta.edu

† Corresponding author: yaodaox@mail.sysu.edu.cn

TABLE I. Copper based spin-1/2 kagomé antiferromagnetic materials. Ordering wave vector for each compound is $\mathbf{q} = \mathbf{0}$. Unavailable values are indicated by a dash. The resonant inelastic x-ray scattering operator formalism developed in this article is applicable generally across different compounds and phases of matter. The magnon and bimagnon scattering operators developed in this article can be applied to these compounds.

Material	$T_N(K)$	Space group	Interaction	Reference
Vesignieite $\text{BaCu}_3\text{V}_2\text{O}_8(\text{OH})_2$	9	$\text{C}2/\text{m}$	$J_1 = 53K, D_p/J_1 = 0.19, D_z/J_1 = 0.07$	[14, 15]
β -Vesignieite $\text{BaCu}_3\text{V}_2\text{O}_8(\text{OH})_2$	9	$\text{R}3\text{m}$	$J = 55K, D = 6K$	[31]
Sr- Vesignieite $\text{Cu}_3\text{SrV}_2\text{O}_8(\text{OH})_2$	11	$\text{P}3_1\text{2}1$	—	[16, 17]
Cd-Kapellasite $\text{CdCu}_3(\text{OH})_6(\text{NO}_3)_2 \cdot \text{H}_2\text{O}$	4	$\text{P}-3\text{m}1$	$J = 45K, D = 4K$	[32]
Edwardsite $\text{CdCu}_3(\text{SO}_4)_2(\text{OH})_6 \cdot 4\text{H}_2\text{O}$	4.3	$\text{P}2_1/\text{c}$	$J = 51K, D_z \gtrapprox 0.1J$	[18]
$\text{YCu}_3(\text{OH})_6\text{Cl}_3$	15	$\text{P}-3\text{m}1$	—	[33]

Raman scattering can be used to detect four-spin correlation, it has a very limited scope, being restricted to $\mathbf{q} \approx \mathbf{0}$. It is known that DM interaction can induce long range magnetic order in kagomé antiferromagnets. There is a quantum critical point at $D/J = 0.1$, where J (D) is the exchange (out-of-plane DM) interaction strength in the Heisenberg model on a kagomé lattice [42]. When the in-plane DM interaction is also taken into account, there are two magnetic ordered phases with a $\mathbf{q} = \mathbf{0}$ structure [43]. Later, in the discussion section we will put our results in the broader context of the classical phase diagram. The positive vector chiral phase where the spins cant out of the kagomé plane is called the umbrella ordered state [7]. The other is the negative vector chiral phase where the spins are still coplanar. Among the antiferromagnetically ordered insulating materials, the positive vector chiral ordered phase is observed more abundantly. However, there are very few negative chiral ordered phases. Two of them are $\text{CdCu}_3(\text{OH})_6(\text{NO}_3)_2 \cdot \text{H}_2\text{O}$ [32] and $\text{YCu}_3(\text{OH})_6\text{Cl}_3$ [33].

In this article, we develop a site symmetry respected theoretical formalism to compute resonant inelastic x-ray scattering (RIXS) spectrum. Using this approach we study the one- and two-site RIXS contribution. The one-site effective scattering operator was constructed from group theoretical arguments. Our approach, valid for a wide range of realistic materials, was applied to the case of an umbrella ordered vector chiral kagomé material vesignieite $\text{BaCu}_3\text{V}_2\text{O}_8(\text{OH})_2$. We calculated the L and K -edge magnon and bimagnon RIXS spectrum of vesignieite $\text{BaCu}_3\text{V}_2\text{O}_8(\text{OH})_2$ arising out of the one- and two-site RIXS operator, respectively. Based on our calculations we show that RIXS has an advantage over inelastic neutron scattering. We can utilize the polarization dependence of the RIXS spectrum to distinguish magnon branches. At the K -edge, we explicitly considered spin-orbit coupling in the Shastry-Shraiman formalism to derive the two-site effective RIXS scattering operator for the bimagnon excitation. We found that a term proportional to vector spin chirality correlation can occur in the RIXS spectrum. Thus, in contrast to inelastic neutron scattering a four spin vector chiral correlation function in the two-site contribution can be detected by RIXS. We also compare our results to Raman to showcase the relative advantage of RIXS. Based on our calculations, we propose that the vector chiral correlation functions can be accessed by current L and K -edge RIXS experiments (within

current resolution limits).

RESULTS

In an umbrella ordered state the spins cant-out of the plane which manifests as a weak out-of-plane ferromagnetic moment, see Fig. 1. Broken mirror symmetry of the kagomé plane [44], which is very common in these materials, see Fig. 1, results in an in-plane DM interaction component \mathbf{D}_p . The umbrella ordering pattern is a consequence of the in-plane interaction. The ligand atoms surrounding the magnetic atom usually form a tilted crystal field. The presence of \mathbf{D}_p , which breaks the rotational symmetry around the c -axis, is necessary to explain the spin wave gaps at the high symmetry points [44]. The degeneracy of positive and negative vector chirality in $\mathbf{q} = \mathbf{0}$ type order is lifted by the out-of-plane DM interaction component \mathbf{D}_z . The sign of D_z selects one of the chiral patterns. The phase diagram of $J - D_z$ is symmetric for positive and negative chirality phase, but it is asymmetric once D_p is taken into account [43]. In this article, we consider positive chirality which is common for a $\mathbf{q} = \mathbf{0}$ type order in a kagomé antiferromagnet such as jarosite and vesignieite.

We consider the following Heisenberg Hamiltonian

$$H = J_1 \sum_{\langle i,j \rangle} \mathbf{S}_i \cdot \mathbf{S}_j + J_2 \sum_{\langle\langle i,j \rangle\rangle} \mathbf{S}_i \cdot \mathbf{S}_j + \sum_{\langle i,j \rangle} \mathbf{D}_{ij} \cdot (\mathbf{S}_i \times \mathbf{S}_j), \quad (1)$$

on the kagomé lattice. Here J_1 (J_2) denotes nearest-neighbor (next nearest-neighbor) antiferromagnetic super-exchange interaction, respectively. The DM interaction term \mathbf{D}_{ij} can be written as $\mathbf{D}_{ij} = -D_p(\mathbf{n}_i + \mathbf{n}_j) + D_z \mathbf{z}^0$, where $\mathbf{n}_i = \sin \alpha_i \mathbf{x}^0 + \cos \alpha_i \mathbf{y}^0$. The sublattice dependent angles α_i are given by $\alpha_1 = 2\pi/3$, $\alpha_2 = 0$, and $\alpha_3 = 4\pi/3$. The order of sites i and j in the DM term is specified in Figure 1(b), that is clockwise in every triangular plaquette. Our choice of the model is motivated by the fact that it is general enough to encompass a host of kagomé materials [44–49], see Table I.

The RIXS cross-section is computed using the Kramers-Heisenberg equation given by [37, 41]

$$\frac{d^2\sigma}{d\omega d\Omega} \propto \sum_f |A_{fi}|^2 \delta(\omega - \omega_{fi}). \quad (2)$$

The transition amplitude

$$A_{fi} = \left\langle f \left| \hat{D}_{out} \frac{1}{\omega_{in} - \hat{H} - i\Gamma} \hat{D}_{in} \right| i \right\rangle, \quad (3)$$

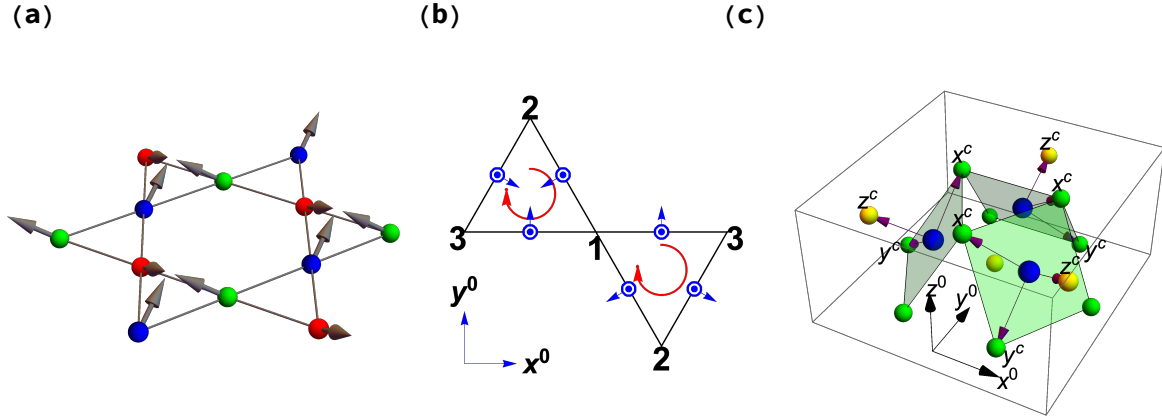


FIG. 1. Kagomé lattice with umbrella ordered spin arrangement. The global kagomé plane coordinate system (x^0, y^0, z^0) and the crystal field coordinate system (x^c, y^c, z^c) are shown. The 2D kagomé plane is set to $x^0 - y^0$. Blue spheres denote copper atoms. Yellow and green denote oxygen atoms. (a) Umbrella order where the spins align out of the kagomé plane with a canting angle. (b) Sublattice indices are denoted by 1, 2, and 3. Out-of-plane component and the in-plane component of the DM interaction are indicated by the circles and the arrows on the bonds, respectively. The order of i and j in the DM interaction is clockwise in every triangular plaquette. (c) Crystal structure of β -vesignieite $\text{BaCu}_3\text{V}_2\text{O}_8(\text{OH})_2$ created from atomic coordinate data [31].

contains the the dipole transition operator \hat{D}_{in} (\hat{D}_{out}) which depend on the incoming (outgoing) momentum \mathbf{q}_{in} (\mathbf{q}_{out}) and the incoming (outgoing) photon polarization ε (ε'), respectively. The dynamics of the scattering operator $\hat{D}_{out} \frac{1}{\omega_{in} - \hat{H} - i\Gamma} \hat{D}_{in}$ is complicated. To consider core hole effects in the intermediate state, the RIXS transition operator in the transition amplitude is typically replaced with an effective scattering operator. Thus, we have $A_{fi} = \langle f | \hat{O}_q | i \rangle$, where $\mathbf{q} = \mathbf{q}_{in} - \mathbf{q}_{out}$ is the transfer momentum. The effective operator provides a tractable analytical approach which captures the essential physics within a suitable approximation formalism. In this paper we use group theory and the Shastry-Shraiman formalism [27] to compute the RIXS intensity.

In general, the effective RIXS scattering operator can be written as [50]

$$\hat{O}_q = \sum e^{i\mathbf{q} \cdot \mathbf{R}_i} (\hat{O}_i + \hat{O}_{ij} + \dots), \quad (4)$$

where the summation is performed over site indices i, j, \dots , etc. The operators are classified according to the number of sites involved in the x-ray scattering process. These operators must be constructed to respect the local site symmetry, the lattice symmetry, and also reflect the core-hole effect to describe elementary excitations in different cases, such as magnon [39, 51], two magnon [41, 52], orbiton [50], and spin-orbital excitation [53]. At zero temperature, the RIXS intensity is computed as

$$I(\mathbf{q}, \omega) = -\frac{1}{\pi} \text{Im} \int_{-\infty}^{\infty} dt e^{i\omega t} (-i) \langle T \hat{O}_q^\dagger(t) \hat{O}_q(0) \rangle, \quad (5)$$

where $\hat{O}_q = \frac{1}{\sqrt{N}} \sum_i e^{i\mathbf{q} \cdot \mathbf{r}_i} \hat{O}_i$ and N is the total number of sites.

The one-site process is the main contribution at the L -edge, where the dominant virtual processes originate from photon-induced intrasite electron hops [30, 37]. As \hat{O}_i is a local operator, it should be invariant under site symmetry operations [50, 53, 54]. In general, for a (pseudo) spin system,

which includes pure spins, an orbital system, and also spin-orbital coupled variables, the single-site operator \hat{O}_i can be written as [39, 50, 53]

$$\hat{O}_i = \sum_{\Gamma_n} \sum_j \alpha_{\Gamma_n, j} P^{\Gamma_n, j} T^{\Gamma_n, j}. \quad (6)$$

In the above, Γ_n denotes an irreducible representation, j denotes the component of group representation, and $\alpha_{\Gamma_n, j}$ is a material dependent coefficient which carries the dipole transition information. $P^{\Gamma_n, j}$ is the polarization factor. $T^{\Gamma_n, j}$ is a combination of symmetry respected angular momentum operators. Both $P^{\Gamma_n, j}$ and $T^{\Gamma_n, j}$ form the basis for Γ_n representation.

The one-site operator is material dependent. Thus, we adopt a specific material to proceed further with our analysis. From Table. I, we choose vesignieite $\text{BaCu}_3\text{V}_2\text{O}_8(\text{OH})_2$ whose copper atoms form a nearly perfect kagomé lattice. The bond length difference between two inequivalent Cu^{2+} site is small [14, 15]. Moreover, it has been suggested that β -vesignieite $\text{BaCu}_3\text{V}_2\text{O}_8(\text{OH})_2$ has a perfect kagomé structure [31]. In our calculations we use the D_p and D_z parameters from Ref. 14 of vesignieite and the atomic coordinate data of β -vesignieite from Ref. 31. Henceforth, we just call the compound vesignieite.

In vesignieite, the octahedron surrounding the Cu^{2+} ion is compressed along the local z -axis of the crystal field. The octahedra tilt from the local z -axis making an angle $\gamma = 26^\circ$ with the kagomé plane [15]. Atomic coordinate data from Ref. [31] suggests that the crystal field belongs to the D_{4h} point group. The hole occupies the d_{z^2} orbital [14, 15], which makes the compressed D_{4h} octahedral crystal field approximation self-consistent. Thus, using Eq. (6), we can write the RIXS scattering operator \hat{O}_i in D_{4h} symmetry as

$$\begin{aligned} \hat{O}_i = & \alpha_{A_{2u}} (\varepsilon_x'^* \varepsilon_y^c - \varepsilon_y'^* \varepsilon_x^c) J_z^c + \alpha_{E_{u,1}} (\varepsilon_z'^* \varepsilon_x^c - \varepsilon_x'^* \varepsilon_z^c) J_y^c \\ & + \alpha_{E_{u,2}} (\varepsilon_y'^* \varepsilon_z^c - \varepsilon_z'^* \varepsilon_y^c) J_x^c, \end{aligned} \quad (7)$$

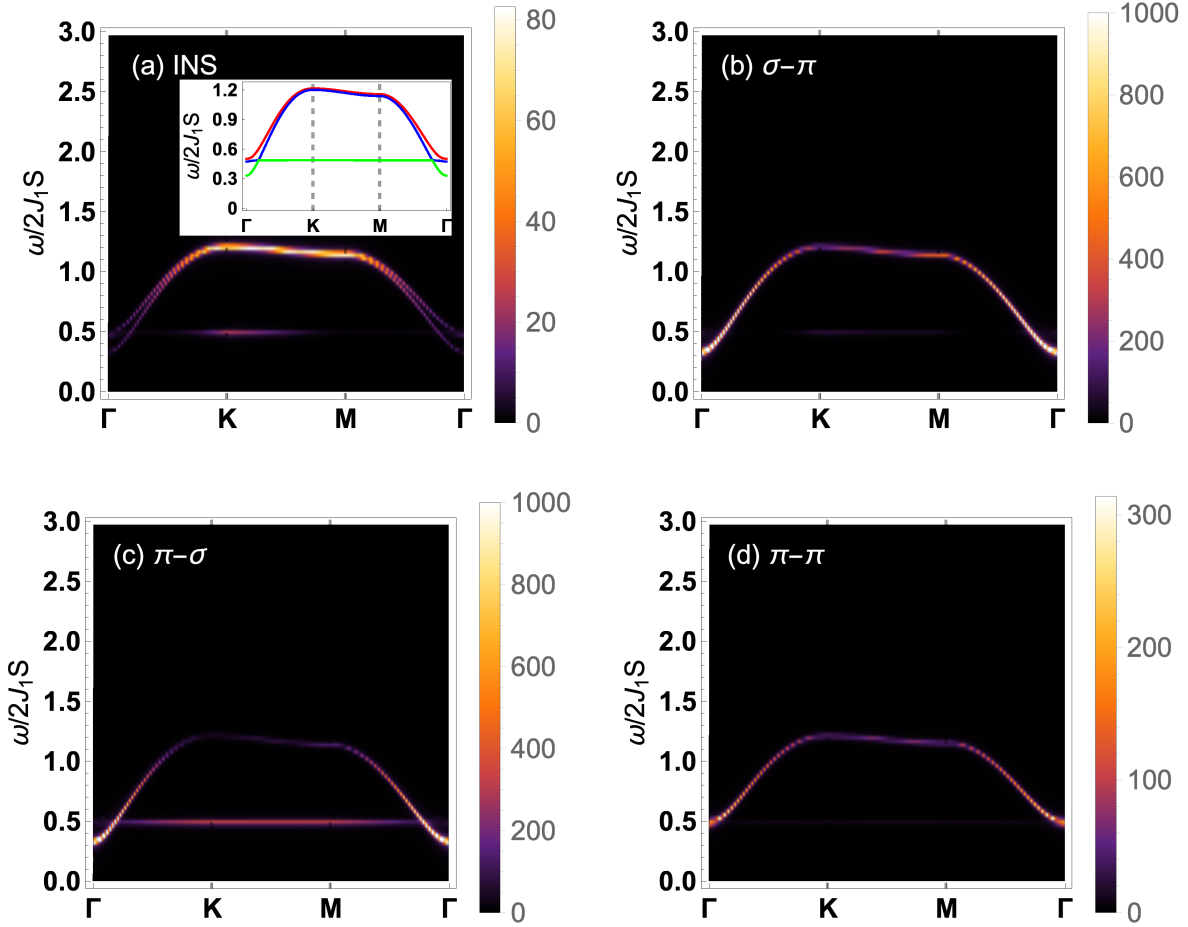


FIG. 2. Magnon excitation in $S = 1/2$ kagomé β -vesignieite $\text{BaCu}_3\text{V}_2\text{O}_8(\text{OH})_2$. (a) Inelastic neutron scattering (INS) spectrum. Magnon dispersion is shown in the inset. (b) – (c) show in-out polarization dependence of one-site Cu L_3 edge resonant inelastic x-ray scattering spectrum. (b) $\sigma_{in} - \pi_{out}$ polarization. (c) $\pi_{in} - \sigma_{out}$ polarization. (d) $\pi_{in} - \pi_{out}$ polarization. ω represents energy transfer in meV. J_1 represents nearest-neighbor exchange energy in meV.

with terms linear in angular momentum operators. We ignore the constant terms since they do not contribute to the inelastic scattering. In the above expression ϵ' (ϵ) represents the outgoing (incoming) photon polarization variables. The superscript c implies an operator written in the crystal field coordinate system. It is possible to rewrite Eq. (7) as $c_i(\epsilon'^*c \times \epsilon^c)_i J_i^c$. Hence, this operator vanishes when ϵ'^*c and ϵ^c are parallel to each other. For the material that we have considered, or other materials, in which spin-orbit coupling is small, we can replace J with S . Based on above considerations, the L_3 -edge one-site operator is given by

$$\hat{O}_i = \frac{4i}{3}(\epsilon_y'^*c \epsilon_z^c - \epsilon_z'^*c \epsilon_y^c)S_x^c + \frac{4i}{3}(\epsilon_x'^*c \epsilon_z^c - \epsilon_z'^*c \epsilon_x^c)S_y^c - \frac{2i}{3}(\epsilon_x'^*c \epsilon_y^c - \epsilon_y'^*c \epsilon_x^c)S_z^c. \quad (8)$$

It is vital to note that the effective one-site RIXS scattering operator was constructed purely based on local site symmetry. The geometry of the lattice and the magnetic order was not important in constructing it. This implies that this operator

can be applied to study other materials with the same local symmetry and different magnetic phases.

The linear photon polarization $\sigma(\pi)$ is perpendicular (parallel) to the scattering plane, see Fig. 3 in Supplementary Information for RIXS experimental geometry set up. The polarization and transferred momentum can be tuned by varying the angle of incidence. We set the scattering angle between the incoming photon and outgoing photon to 130° . For vesignieite case, it can be found that the entire first Brillouin zone can be comprehensively covered in a RIXS experiment using our proposed experimental setup as outlined in the Supplementary Information.

Using parameters for vesignieite [14], $D_p/J_1 = 0.19$, $D_z/J_1 = 0.07$, and $J_2 = 0$, the dynamical structure factor (DSF). We define the dynamical structure factor as $\sum_{\alpha\beta}(\delta_{\alpha\beta} - \hat{q}_\alpha \hat{q}_\beta)S^{\alpha\beta}(\mathbf{q}, \omega)$, where $S^{\alpha\beta}(\mathbf{q}, \omega) = \int_{-\infty}^{\infty} \frac{dt}{2\pi} \langle S_\alpha^\alpha(t)S_{-\mathbf{q}}^\beta(0) \rangle e^{i\omega t}$ and α, β refers to x, y , and z . The unit vector component in the direction of q is denoted by \hat{q} . To be consistent with INS we have projected out the longitudinal momentum component. Since we are missing form-factors in front of our dy-

namical structure factor, this expression is not exactly equal to INS.

In Fig. 2 we show the one-site contribution results at the L_3 -edge. Since σ polarization is perpendicular to the scattering plane, we can infer from Eq. (8) that the contribution from the $\sigma_{in} - \sigma_{out}$ channel is zero. In the total DSF plot, Fig. 2(a), the middle band (blue band) in the inset of Fig. 2(a) and the highest band (red band) almost merge together when $\omega > 0.8J_1S$. Furthermore, the spectral weight is small around Γ point. These features make it hard to extract the complete dispersion from INS [13]. From the L_3 -edge RIXS spectra with different polarization combination, Fig. 2(b) – Fig. 2(d), it is clear that x-ray polarization channels are sensitive to a varying degree. The $\sigma_{in} - \pi_{out}$ channel is most sensitive to the middle (blue) band with a very small spectral weight for the lowest (green) band. However, the spectral weight in the green band is enhanced in $\pi_{in} - \sigma_{out}$ channel, and the $\pi_{in} - \pi_{out}$ channel mainly detects the red band. Based on our calculations, we demonstrate that L_3 -edge RIXS with different polarization combination can differentiate and extract the complete dispersion. This is an experimental advantage over INS.

The two-site term in Eq. (4) is the leading contribution at the Cu K -edge RIXS, since spin-orbital coupling is absent for $1s$ electrons. Thus, a one-site single spin flip excitation is forbidden in this case. We use the dipole transition operator in D_{4h} crystal field symmetry given by $\hat{D}_{in} = \varepsilon_x p_x^\dagger s + \varepsilon_y p_y^\dagger s$ in the Kramers-Heisenberg amplitude Eq. (3). The most important feature of the intermediate state core-hole is the modification of the super-exchange process [41, 52, 55]. Thus, the effect of core-hole dynamics in the intermediate state is important [55]. Hence, it is necessary to carefully consider for a Mott insulator how the virtual hopping processes are modified by the core hole. Thus, we use the Shastry-Shraiman formalism [27, 30].

We can generalize the RIXS formalism to include spin-orbit coupling at the K -edge during the virtual hopping process. The full intermediate state Hamiltonian is given by $H = H_t + H_U + H_{pho}$, where H_t is the electron hopping part, H_U is the Hubbard interaction, and H_{pho} is the pure photon part [56, 57]. The presence of spin-orbital coupling introduces a non-abelian phase in the hopping amplitude. Thus, we have $H_t = \sum_{i,j,\sigma} b_{ij} c_{i\sigma}^\dagger c_{j\sigma} + \sum_{i,j,\sigma,\sigma'} c_{i\sigma}^\dagger [\mathbf{C}_{ij} \cdot \boldsymbol{\sigma}]_{\sigma\sigma'} c_{j\sigma'}$, where $\boldsymbol{\sigma}$ is the Pauli matrix vector. \mathbf{C}_{ij} is purely imaginary since spin-orbital coupling is time reversal invariant. We set $\mathbf{C}_{ij} = \mathbf{i}\mathbf{n}_{ij}|\mathbf{C}_{ij}|$, where \mathbf{n}_{ij} is an unit vector related to the spin-orbit coupling. The hopping part can then be recasted to a familiar form $H_t = \sum_{ij} t_{ij} \mathbf{c}_i^\dagger \mathbf{A}_{ij} \mathbf{c}_j$, where $\mathbf{c}_j = (c_{j\uparrow}, c_{j\downarrow})^T$ with $t_{ij} \cos \theta_{ij} = b_{ij}$, $t_{ij} \sin \theta_{ij} = |\mathbf{C}_{ij}|$, and $\mathbf{A}_{ij} = e^{i\theta_{ij}\mathbf{n}_{ij}\cdot\boldsymbol{\sigma}}$ (a 2×2 matrix). Next, since we are considering a Mott insulator case where $t \ll U$, we can regard H_t as a perturbation [27, 30]. Thus, we have

$$\begin{aligned} \hat{O} &= \hat{D}_{out} \frac{1}{\omega_{in} - \hat{H} - i\Gamma} \hat{D}_{in} \\ &= \hat{D}_{out} \frac{1}{\omega_{in} - \hat{H}_U - \hat{H}_{pho} - i\Gamma} \sum_{n=0}^{\infty} \left(\frac{\hat{H}_t}{\omega_{in} - \hat{H}_U - \hat{H}_{pho} - i\Gamma} \right)^n \hat{D}_{in}. \end{aligned} \quad (9)$$

Thus, the leading inelastic x-ray scattering term ($n = 2$) can

be written as

$$\hat{O}_{\mathbf{q}} = \eta_c \sum_{i,j} e^{i\mathbf{q}\cdot\mathbf{r}_i} [J_{ij} \mathbf{S}_i \cdot \mathbf{S}_j + \mathbf{D}_{ij} \cdot (\mathbf{S}_i \times \mathbf{S}_j)], \quad (10)$$

with the polarization factor $\varepsilon_x^{*\prime} \varepsilon_x + \varepsilon_y^{*\prime} \varepsilon_y^{*}$. The exchange and DM interaction modification factor η_c is a function of the core-hole potential U_c and U , see Supplementary Information. We used Eq. (10) to calculate the results in Fig. 4.

For a comprehensive understanding, we also show the ultrashort core-hole lifetime (UCL) approximation derivation [41, 52] of the RIXS operator Eq. 10 in Supplementary Information. In general, for a Mott insulator the condition $H_t \ll \omega_{in} - H_U - H_{pho} - i\Gamma$ needs to be obeyed. Thus, the Shastry-Shraiman formalism, which is based on the above condition, is a more natural expansion scheme compared to UCL. The UCL approximation is a sufficient but not necessary condition. Thus, the Shastry-Shraiman approach is the more general scheme.

Note, in our formalism, the one-site RIXS operator corresponds to the $n = 0$ term [30]. The one-site operator group theory inspired construction is general enough to allow higher order (multiple) terms beyond the linear spin operator dipole transition terms in the RIXS operator. But the Shastry-Shraiman formalism is restricted to the dipole approximation implicitly. Practically, it is hard to calculate a multipole contribution in the Shastry-Shraiman formalism.

The kagomé material β -vesignieite belongs to the D_{3d} point group. Thus, an effective two-site scattering operator Eq. (10) corresponds to the A_{1g} irreducible representation. Using the Shastry-Shraiman formalism we can derive the Raman scattering operator (which corresponds to a two-site term) expression as

$$\hat{O}_{\text{Raman}} \propto \sum_{ij} \frac{(\boldsymbol{\epsilon}^{*\prime} \cdot \boldsymbol{\delta})(\boldsymbol{\epsilon} \cdot \boldsymbol{\delta})}{\omega_i - U} [J_{ij} \mathbf{S}_i \cdot \mathbf{S}_j + \mathbf{D}_{ij} \cdot (\mathbf{S}_i \times \mathbf{S}_j)], \quad (11)$$

which has three channels A_{1g} , $(E_g, 1)$, and $(E_g, 2)$. The contribution to the elastic channel comes from A_{1g} . See Supplementary Information for details.

Both the RIXS and the Raman processes measure a four spin correlation function. Whereas Raman is restricted mainly to $\mathbf{q} \approx \mathbf{0}$, RIXS has the ability to comprehensively explore the Brillouin zone for all energy scales (resolution and scattering geometry permitting). The two-site RIXS intensity can be divided into three parts. First, the exchange part I^E is $\sim \langle (JS_k \cdot S_l), (JS_i \cdot S_j) \rangle$. The second chiral DM part I^D contribution is $\sim \langle \mathbf{D} \cdot (\mathbf{S}_k \times \mathbf{S}_l), \mathbf{D} \cdot (\mathbf{S}_i \times \mathbf{S}_j) \rangle$. Finally, we have a mixed contribution I^M coming from the overlap of the exchange and the chiral DM part. The chiral contribution measures the projection of the vector chirality correlation function, which is currently inaccessible from a direct measurement [23, 24]. Moreover, in the umbrella order state, the scalar chirality is proportional to the vector chirality [26] since $\langle \mathbf{S}_i \cdot (\mathbf{S}_j \times \mathbf{S}_k) \rangle \approx \langle \mathbf{S}_i \rangle \cdot \langle \mathbf{S}_j \times \mathbf{S}_k \rangle$. Thus, the I^D part carries information related to the six-spin scalar chiral correlation function.

The two-site RIXS intensity is shown in Fig. 3. It can be proved that all physically meaning RIXS intensities are non-

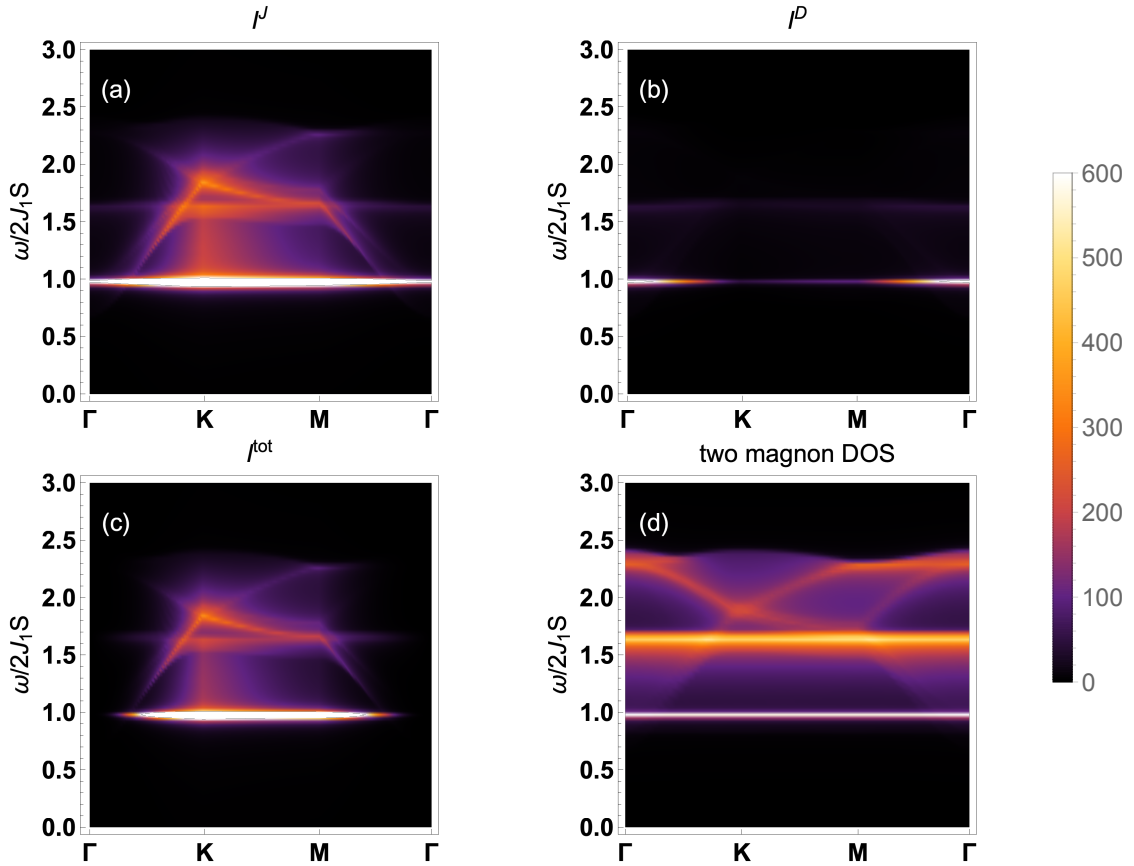


FIG. 3. Two-site RIXS spectra in vesignieite. The total spectrum consist of the exchange I^J part, the Dzyaloshinskii-Moriya I^D part which is proportional to vector chiral correlation, and the mixed I^m part. (a) I^J , (b) I^D , (c) the total spectrum $I = I^D + I^J$, and (d) two magnon density of states, $D(\mathbf{q}, \omega)$.

negative. The mixed part is real but with both positive and negative intensity contribution. According to the definition of RIXS intensity Eq. (5), only the correlation functions which have the form $\langle T\hat{b}(t)\hat{b}(t)\hat{b}^\dagger(0)\hat{b}^\dagger(0)\rangle$ contribute at zero temperature, where \hat{b} is the Bogoliubov quasiparticle operator. This implies, we only require the $\hat{b}^\dagger\hat{b}^\dagger$ terms in \hat{O}_q . Thus, at the Γ point where $\mathbf{q} = \mathbf{0}$, the two-site operator Eq. (10) reduces to the Hamiltonian. Since Bogoliubov transformation eliminates the $\hat{b}\hat{b}$ and $\hat{b}^\dagger\hat{b}^\dagger$ terms in the Hamiltonian, the two-site intensity is identically zero at $\mathbf{q} = \mathbf{0}$, see Fig. (3)(c). This argument provides a simple proof for identically zero intensity signal at the Γ point for a two-site contribution. Our argument is also valid in other cases also [52, 58, 59]. Thus, at this point the intensity $I^J + I^D = -I^m$. Although the RIXS intensity is zero at the Γ point, information on the two-magnon excitation at zero wave vector can be extracted from two-magnon Raman scattering. Here, since we calculate the non-interacting case, the spectra of the two-site contribution has the same shape as the two-magnon density of states $D(\mathbf{q}, \omega) = \sum_{\mathbf{k}, m, n} M \delta(\omega - \omega_{mk} - \omega_{nq-k})$.

DISCUSSION

Our calculations suggest that the cross section at the L -edge RIXS is not simply proportional to DSF [60, 61]. It is obvi-

ous that the spectral weight distribution in DSF and in RIXS are different in Fig. 2. The spin operator in the effective one-site RIXS operator Eq. (8) is determined from the local symmetry. In the local crystal field coordinate system, this means that the single magnon can be detected in Cu L -edge RIXS [39, 51]. After rotation of the spin operator and the polarization, the effective operator can be written as $O_i = A(\mathbf{q}, \alpha_i)S_i^x + B(\mathbf{q}, \alpha_i)S_i^y + C(\mathbf{q}, \alpha_i)S_i^z$ with momentum dependent coefficients A , B , and C . These relationships are too complicated to be listed in the main text. We describe the procedure to obtain them in Supplementary Information

In the magnetic ordered phase, the leading RIXS contribution is $I_{\text{RIXS}} \sim \sum_n M(\mathbf{q})\delta(\omega - \omega_{nq})$ where n is the band index, ω_{nq} is the magnon dispersion, and $M(\mathbf{q})$ is the RIXS matrix element. So, the overall shape of the spectrum are along the dispersion. In a tetragonal system with a collinear magnetic order such as a cuprate, the local z axis of the crystal field coincides with the global z axis. The spins lie in the $x - y$ plane. So, the rotation of the spin operator in the effective one-site RIXS operator is the same as in DSF [39]. Thus, RIXS can have very similar spectral weight as in DSF [39, 51]. But in the kagomé material with non-collinear magnetic order studied here, these rotations make RIXS totally different from DSF. Essentially, L -edge RIXS relies on the

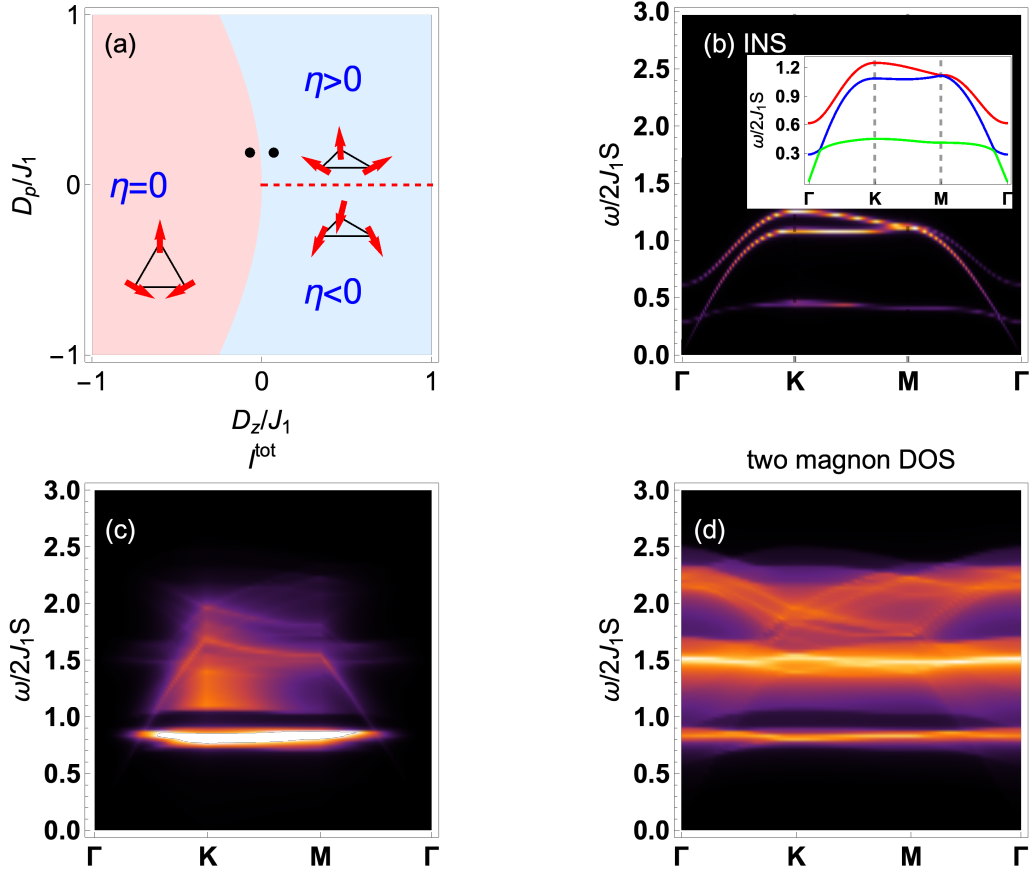


FIG. 4. Phase diagram and resonant inelastic x-ray scattering response of negative vector chiral phase. (a) The classical phase diagram of kagomé antiferromagnet. The blue (red) region indicates the positive (negative) vector chiral phases. The spins in the positive vector chiral phase cant out of the kagomé plane when $D_p \neq 0$. The red dashed line represents coplanar positive vector chiral phase with $D_p = 0$. The spins in the negative vector chiral phase is coplanar. The parameters of the black points are $D_p = 0.19J_1$, $D_z = \pm 0.07J_1$, vesigneite is in the point with positive D_z . (b) INS spectrum ,(c) two site RIXS spectrum, (d) two magnon density of state of the negative vector chiral phase with $D_p = 0.19J_1$, $D_z = -0.07J_1$.

spin-orbit coupling of the core states which makes RIXS different from DSF. One can consider magnon-magnon interaction which is known to have significant renormalization effect on the frustrated kagomé antiferromagnet [45]. In this case we replace the free magnon propagator by the renormalized one in Eq. (5) to include this effect. However, this modification and considering any potential magnon decay effects will not change the main conclusions of this article.

We discuss the vector chiral RIXS correlation contribution I^D . We derived Eq. (10) by considering virtual hopping in the core-hole modified super-exchange process. The antisymmetric exchange term is always allowed by symmetry in the lattice without bond inversion center. So, it is natural to include this term in the general kagomé material, even with weak spin-orbital coupling. For other lattice configurations, such as the triangular lattice, the honeycomb lattice, and even the square lattice, this antisymmetric exchange can exist for some materials. The polarization sensitivity is introduced in the photon

absorbing and emitting process at the core hole site. Hence, the exchange and the DM term has the same polarization dependent factor.

The degeneracy of the positive and negative vector chiral state is lifted by DM interaction which is intrinsic to the material. Here we discuss the difference between the spectrum of the positive and the negative vector chiral state. In Fig. 4(a), we show our computed classical phase diagram of the $J_1 - D_z - D_p$ model [43]. The negative vector chiral phase is always coplanar. But, the positive vector chiral phase is coplanar only when $D_p = 0$. Since there are very few insulating negative vector chiral kagomé materials [32, 33] and parameters are unavailable (presently), we choose $D_p = 0.19J_1$ and $D_z = -0.07J_1$ for the negative vector chiral β -vesigneite. These two parameter sets are denoted by the black points in the Fig. 4(a). The INS spectrum, the two-site RIXS intensity, and two-magnon density of state of this negative vector chiral phase are shown in Figs. 4(b) – (d). In contrast to positive

chiral materials (Fig. 2(a)), the spin wave dispersion of this phase is gapless. So when $D_p \neq 0$, which is a common feature in broken mirror symmetry kagomé planes, the negative vector chiral phase is gapless. When $D_p = 0$, both chiral phase are coplanar ($\eta = 0$) and gapless, they correspond to $\pm D_z$. We can identify the difference between the positive and the negative vector chiral state using $\sin(\alpha_i - \alpha_j)$ (even though at the linear level this distinction is not apparent).

The exchange and chiral part of our RIXS contribution can be separated experimentally. Here, we consider two proposals to study this vector chiral correlation in RIXS. Chiral correlation can have higher critical temperature than the spin correlation [11, 62–64]. Thus, chiral correlations can be studied around the magnetic critical ordering temperature where the spin correlation is suppressed, but the chiral correlation survives. Another proposal is based on the spin current interpretation of vector chirality[8, 25, 26]. It has been pointed out that electric polarization is proportional to the vector chirality. Thus, vector chirality can be tuned by an external electric field.

Our predicted RIXS intensity features can be verified experimentally within the current state-of-the-art RIXS resolution, which is of the same order of magnitude [3, 65]. For example, consider the magnetically ordered kagomé materials outlined in Table. I, and jarosite [13, 48] which have $J \sim 5$ meV. Thus, the one-site RIXS spectrum has an energy of the order of $\sim 2J_1S \sim 10$ S meV, see Fig. (2). This energy is around 5 meV for a $S = 1/2$ material and 25 meV for $S = 5/2$ material. Similarly, the two-site RIXS spectrum is $\sim 3J_1S \sim 15$ S meV. Thus, the energy is around 7.5 meV for $S = 1/2$ and 37.5 meV for $S = 5/2$. We hope these resolution estimates and the results in our current paper will encourage RIXS experimentalists to study the kagomé materials family.

In this article, we studied the L and K -edge RIXS features of an umbrella ordered kagomé antiferromagnet. Considering the one- and two-site RIXS contribution we have evaluated the magnon and bimagnon contributions, respectively. We have used a general site symmetry respected method to construct the one-site effective RIXS operator which can be used to study spin, orbital, and spin-orbital excitations. We revealed that the one-site contribution in the L -edge RIXS can be entirely different from the DSF. Considering vesignieite as an example, we showed that the magnon dispersion of vesignieite can be easily distinguished using different combinations of incoming and outgoing x-ray polarization photons. We also derived the two-site effective RIXS operator at the K -edge in the presence of DM interaction (considering spin-orbit interaction). Utilizing a Shastry-Shraiman formalism that incorporates spin-orbit coupling, we calculate the vector chiral correlation contributions at K -edge RIXS. We compare and contrast our RIXS findings with those of INS and Raman. We provide two proposals to separate the vector chiral correlation in the total RIXS spectrum. Finally, we note that our RIXS operator construction formalism should apply to non-coplanar non-collinear magnetic ordering on lattices beyond the kagomé case [66].

METHODS

Linear spin wave theory

We use spin wave theory to study dynamic vector chirality of the magnetically ordered $\mathbf{q} = \mathbf{0}$ phase of antiferromagnetic kagomé materials. To carry out the calculation, it is necessary to express the spin operators in the local moment coordinate system as

$$\begin{aligned} S_i^{x^0} &= S_i^x \cos \alpha_i + S_i^y \sin \alpha_i \sin \eta + S_i^z \sin \alpha_i \cos \eta, \\ S_i^{y^0} &= -S_i^x \sin \alpha_i + S_i^y \cos \alpha_i \sin \eta + S_i^z \cos \alpha_i \cos \eta, \\ S_i^{z^0} &= -S_i^y \cos \eta + S_i^z \sin \eta, \end{aligned} \quad (12)$$

where α_i are sublattice dependent angles $\alpha_1 = 2\pi/3$, $\alpha_2 = 0$ and $\alpha_3 = 4\pi/3$ for the three sublattices respectively, see Fig. 1; $\alpha_1 = 4\pi/3$, $\alpha_2 = 0$ and $\alpha_3 = 2\pi/3$ for the negative vector chiral phase, see Fig. 4 (a). The canting angle is η , where $\eta = 0$ corresponds to spins in the kagomé basal plane. Next, we perform Holstein-Primakoff transformations at the linear spin wave level using $S_i^z = S - a_i^\dagger a_i$, $S_i^- \approx \sqrt{2S} a_i^\dagger$, $S_i^+ \approx \sqrt{2S} a_i$. The Fourier transformed spin wave Hamiltonian can be obtained using the transformation $a_{\alpha,l} = \frac{1}{\sqrt{N}} \sum_{\mathbf{k}} a_{\alpha,\mathbf{k}} e^{i\mathbf{k} \cdot (\mathbf{R}_l + \rho_a)}$, where ρ_a is the displacement of the α atom in the l -th unit cell. N represents the total number of unit cells. It should be noted that there is no analytical solution even at the linear spin wave level when the canting angle $\eta \neq 0$. Thus, we have performed a numerical Bogoliubov diagonalization transformation of the Hamiltonian. A comprehensive and detailed procedure for diagonalizing the quadratic Hamiltonian is given in the Supplementary Information.

RIXS and Raman operator derivation

Resonant inelastic x-ray scattering and Raman are both photon-in photon-out process. The transition amplitude A_{fi} can be written as

$$A_{fi} = \left\langle f \left| \hat{H}_{coup} \frac{1}{\omega_{in} - \hat{H} - i\eta} \hat{H}_{coup} \right| i \right\rangle, \quad (13)$$

where \hat{H}_{coup} is the light-matter coupling Hamiltonian. In RIXS, the incoming beam is tuned to match the absorption edge of the specific elements to cause the $1s \rightarrow 4p$ transition. In this case \hat{H}_{coup} can be simplified to a dipole transition operator \hat{D} . In Raman, the incoming beam is visible light with several eV energy and close to the Hubbard gap. Thus, \hat{H}_{coup} describes the intersite electron hops coupled to the electromagnetic field of photon. This can be introduced by a Peierls substitution $H_{coup} = \sum_{ij} t_{ij} e^{i \frac{e}{\hbar c} \int_j^i \mathbf{A}(\mathbf{r}) \cdot d\mathbf{l}} \mathbf{c}_i^\dagger \mathbf{A}_{ij} \mathbf{c}_j$. Once \hat{H}_{coup} is determined, the transition amplitude (or the effective scattering operator) can be calculated using perturbation expansion. The electron hopping part in the Hamiltonian \hat{H} is regarded as a perturbation in the Shastry-Shraiman formalism [27]. Then the intermediate state propagator $(\omega_{in} - \hat{H} - i\eta)^{-1}$ can be expanded as stated in the main text (Eq.(9)). We are interested in the low energy excitation so we insert the complete set wave functions of one hole and one double occupied state. Then the electron operator c and c^\dagger can be represented by spin operators and we find a spin Hamiltonian. Full details of the calculation are given in the Supplementary Information.

DATA AVAILABILITY

All relevant data are available from the authors upon request.

REFERENCES

1. L. D. Barron, *Nature Materials* **7**, 691 (2008).
2. S. Bordács, I. Kézsmárki, D. Szaller, L. Demkó, N. Kida, H. Muraoka, Y. Onose, R. Shimano, T. Rőm, U. Nagel, S. Miyahara, N. Furukawa, and Y. Tokura, *Nature Physics* **8**, 734 (2012).
3. S. Mongan, Z. Huang, T. Datta, T. Nomura, and D.-X. Yao, *Scientific Reports* **9**, 12771 (2019).
4. M. O. Yokusuk, H.-S. Kim, K. D. Hughey, J. Kim, A. V. Stier, K. R. O’Neal, J. Yang, S. A. Crooker, K. Haule, S.-W. Cheong, D. Vanderbilt, and J. L. Musfeldt, *npj Quantum Materials* **5** (2020).
5. R. Moessner and A. P. Ramirez, *Phys. Today* **59**, 24 (2006).
6. A. Chubukov, *Phys. Rev. Lett.* **69**, 832 (1992).
7. D. Grohol, K. Matan, J.-H. Cho, S.-H. Lee, J. W. Lynn, D. G. Nocera, and Y. S. Lee, *Nature Materials* **4**, 323 (2005).
8. H. Katsura, N. Nagaosa, and A. V. Balatsky, *Phys. Rev. Lett.* **95**, 057205 (2005).
9. I. A. Sergienko and E. Dagotto, *Phys. Rev. B* **73**, 094434 (2006).
10. M. Mostovoy, *Phys. Rev. Lett.* **96**, 067601 (2006).
11. H. Kawamura, *Journal of Physics: Condensed Matter* **10**, 4707 (1998).
12. M. Ramakrishnan, E. Constable, A. Cano, M. Mostovoy, J. S. White, N. Gurung, E. Schierle, S. d. Brion, C. V. Colin, F. Gay, P. Lejay, E. Ressouche, E. Weschke, V. Scagnoli, R. Ballou, V. Simonet, and U. Staub, *npj Quantum Materials* **4**, 60 (2019).
13. K. Matan, D. Grohol, D. G. Nocera, T. Yildirim, A. B. Harris, S. H. Lee, S. E. Nagler, and Y. S. Lee, *Phys. Rev. Lett.* **96**, 247201 (2006).
14. A. Zorko, F. Bert, A. Ozarowski, J. van Tol, D. Boldrin, A. S. Wills, and P. Mendels, *Phys. Rev. B* **88**, 144419 (2013).
15. M. Yoshida, Y. Okamoto, M. Takigawa, and Z. Hiroi, *Journal of the Physical Society of Japan* **82**, 013702 (2013).
16. D. Boldrin and A. S. Wills, *J. Mater. Chem. C* **3**, 4308 (2015).
17. A. Verrier, F. Bert, J. M. Parent, M. El-Amine, J. C. Orain, D. Boldrin, A. S. Wills, P. Mendels, and J. A. Quilliam, *Phys. Rev. B* **101**, 054425 (2020).
18. H. Ishikawa, Y. Okamoto, and Z. Hiroi, *Journal of the Physical Society of Japan* **82**, 063710 (2013).
19. J.-X. Yin, S. S. Zhang, G. Chang, Q. Wang, S. S. Tsirkin, Z. Guguchia, B. Lian, H. Zhou, K. Jiang, I. Belopolski, N. Shumiya, D. Multer, M. Litskevich, T. A. Cochran, H. Lin, Z. Wang, T. Neupert, S. Jia, H. Lei, and M. Z. Hasan, *Nature Physics* **15**, 443 (2019).
20. N. J. Ghimire and I. I. Mazin, *Nature Materials* **19**, 137 (2020).
21. Z. Hao and O. Tchernyshyov, *Phys. Rev. B* **87**, 214404 (2013).
22. D. Ketenoglu, M. Harder, K. Klementiev, M. Upton, M. Taherkhani, M. Spiwek, F.-U. Dill, H.-C. Wille, and H. Yavaş, *Journal of synchrotron radiation* **22**, 961 (2015).
23. S. V. Maleyev, *Phys. Rev. Lett.* **75**, 4682 (1995).
24. V. P. Plakhty, J. Kulda, D. Visser, E. V. Moskvin, and J. Wosnitza, *Phys. Rev. Lett.* **85**, 3942 (2000).
25. L. N. Bulaevskii, C. D. Batista, M. V. Mostovoy, and D. I. Khomskii, *Phys. Rev. B* **78**, 024402 (2008).
26. K. A. Al-Hassanieh, C. D. Batista, G. Ortiz, and L. N. Bulaevskii, *Phys. Rev. Lett.* **103**, 216402 (2009).
27. B. S. Shastry and B. I. Shraiman, *Phys. Rev. Lett.* **65**, 1068 (1990).
28. W.-H. Ko, Z.-X. Liu, T.-K. Ng, and P. A. Lee, *Phys. Rev. B* **81**, 024414 (2010).
29. P. A. Lee and N. Nagaosa, *Phys. Rev. B* **87**, 064423 (2013).
30. W.-H. Ko and P. A. Lee, *Phys. Rev. B* **84**, 125102 (2011).
31. H. Yoshida, Y. Michiue, E. Takayama-Muromachi, and M. Isobe, *J. Mater. Chem.* **22**, 18793 (2012).
32. R. Okuma, T. Yajima, D. Nishio-Hamane, T. Okubo, and Z. Hiroi, *Phys. Rev. B* **95**, 094427 (2017).
33. A. Zorko, M. Pregelj, M. Gomilšek, M. Klanjšek, O. Zaharko, W. Sun, and J.-X. Mi, *Phys. Rev. B* **100**, 144420 (2019).
34. J. Schlappa, U. Kumar, K. J. Zhou, S. Singh, M. Mourigal, V. N. Strocov, A. Revcolevschi, L. Patthey, H. M. Rønnow, S. Johnston, and T. Schmitt, *Nature Communications* **9**, 5394 (2018).
35. M. Le Tacon, G. Ghiringhelli, J. Chaloupka, M. M. Sala, V. Hinkov, M. W. Haverkort, M. Minola, M. Bakr, K. J. Zhou, S. Blanco-Canosa, C. Monney, Y. T. Song, G. L. Sun, C. T. Lin, G. M. De Luca, M. Salluzzo, G. Khaliullin, T. Schmitt, L. Braicovich, and B. Keimer, *Nat. Phys.* **7**, 725 (2011).
36. M. P. M. Dean, R. S. Springell, C. Monney, K. J. Zhou, J. Pereiro, I. Božović, B. Dalla Piazza, H. M. Rønnow, E. Morenzoni, J. van den Brink, T. Schmitt, and J. P. Hill, *Nat. Mater.* **11**, 850 (2012).
37. L. J. P. Ament, M. van Veenendaal, T. P. Devereaux, J. P. Hill, and J. van den Brink, *Rev. Mod. Phys.* **83**, 705 (2011).
38. C. Jia, K. Wohlfeld, Y. Wang, B. Moritz, and T. P. Devereaux, *Phys. Rev. X* **6**, 021020 (2016).
39. M. W. Haverkort, *Phys. Rev. Lett.* **105**, 167404 (2010).
40. N. Pakhira, J. K. Freericks, and A. M. Shvaika, *Phys. Rev. B* **86**, 125103 (2012).
41. J. van den Brink, *EPL* **80**, 47003 (2007).
42. O. Cépas, C. M. Fong, P. W. Leung, and C. Lhuillier, *Phys. Rev. B* **78**, 140405 (2008).
43. M. Elhajal, B. Canals, and C. Lacroix, *Phys. Rev. B* **66**, 014422 (2002).
44. T. Yildirim and A. B. Harris, *Phys. Rev. B* **73**, 214446 (2006).
45. A. L. Chernyshev and M. E. Zhitomirsky, *Phys. Rev. B* **92**, 144415 (2015).
46. M. Hering and J. Reuther, *Phys. Rev. B* **95**, 054418 (2017).
47. S. A. Owerre, *Phys. Rev. B* **95**, 014422 (2017).
48. P. Laurell and G. A. Fiete, *Phys. Rev. B* **98**, 094419 (2018).
49. Y. Lu, X. Guo, V. Koval, and C. Jia, *Phys. Rev. B* **99**, 054409 (2019).
50. L. J. P. Ament and G. Khaliullin, *Phys. Rev. B* **81**, 125118 (2010).
51. L. J. P. Ament, G. Ghiringhelli, M. M. Sala, L. Braicovich, and J. van den Brink, *Phys. Rev. Lett.* **103**, 117003 (2009).
52. F. Forte, L. J. P. Ament, and J. van den Brink, *Phys. Rev. B* **77**, 134428 (2008).
53. W. M. H. Natori, M. Daghofer, and R. G. Pereira, *Phys. Rev. B* **96**, 125109 (2017).
54. L. Savary and T. Senthil, *arXiv preprint arXiv:1506.04752* (2015).
55. D. S. Ellis, J. Kim, J. P. Hill, S. Wakimoto, R. J. Birgeneau, Y. Shvyd’ko, D. Casa, T. Gog, K. Ishii, K. Ikeuchi, A. Paramekanti, and Y.-J. Kim, *Phys. Rev. B* **81**, 085124 (2010).
56. L. Shekhtman, O. Entin-Wohlman, and A. Aharoni, *Phys. Rev. Lett.* **69**, 836 (1992).
57. S. Zhu, Y.-Q. Li, and C. D. Batista, *Phys. Rev. B* **90**, 195107 (2014).
58. T. Nagao and J.-i. Igarashi, *Phys. Rev. B* **75**, 214414 (2007).
59. C. Luo, T. Datta, Z. Huang, and D.-X. Yao, *Phys. Rev. B* **92**, 035109 (2015).
60. P. Marra, S. Sykora, K. Wohlfeld, and J. van den Brink, *Phys. Rev. Lett.* **110**, 117005 (2013).
61. C. Jia, K. Wohlfeld, Y. Wang, B. Moritz, and T. P. Devereaux, *Phys. Rev. X* **6**, 021020 (2016).
62. D. X. Viet and H. Kawamura, *Phys. Rev. Lett.* **102**, 027202 (2009).

63. S. Okumura, H. Yoshino, and H. Kawamura, *Phys. Rev. B* **83**, 094429 (2011).

64. A. Ruff, P. Lunkenheimer, H.-A. Krug von Nidda, S. Widmann, A. Prokofiev, L. Svistov, A. Loidl, and S. Krohns, *npj Quantum Materials* **4**, 24 (2019).

65. M. Moretti Sala, K. Martel, C. Henriet, A. Al Zein, L. Simonelli, C. Sahle, H. Gonzalez, M.-C. Lagier, C. Ponchut, S. Huotari, *et al.*, *Journal of synchrotron radiation* **25**, 580 (2018).

66. O. A. Starykh, *Reports on Progress in Physics* **78**, 052502 (2015).

Guangdong Special Projects.

AUTHOR CONTRIBUTIONS

T. D, Z. X, and D. X. Y conceived and designed the project. Z. X performed the calculation. T. D. and D. X. Y checked the calculations. All authors contributed to the discussion of the results and wrote the paper.

COMPETING INTERESTS

The authors declare no competing interests.

ADDITIONAL INFORMATION

Supplementary Information is available for the paper at this weblink

Correspondence and requests for materials should be addressed to T. Datta or D. X. Yao.

ACKNOWLEDGEMENTS

We thank W. M. H. Natori and Y. Zeng for helpful discussions. T. D. acknowledges funding support from Sun Yat-Sen University Grant No. OEMT-2017-KF-06. Z. X. and D. X. Y. are supported by NKRDPC-2017YFA0206203, NKRDPC-2018YFA0306001, NSFC-11974432, NSFG-2019A1515011337, National Supercomputer Center in Guangzhou, and Leading Talent Program of